

# Analytical modelling of electromagnetic bulging of thin metallic tubes

SeyedVahid Hosseini<sup>1\*</sup>, Sara Hatami<sup>2</sup>, Abolfazl Darvizeh<sup>2</sup>, Mahmoud Chizari<sup>1</sup>

<sup>1</sup> University of Hertfordshire, Hatfield, AL10 9AB, UK

<sup>2</sup> University of Guilan, Rasht 3756, Iran

\*v.hosseini@herts.ac.uk

**Abstract.** The core goal of this study is to create an analytical method based on the energy balance equation- to model the plastic deformation of thin metallic tubes in a high velocity forming process under axisymmetric conditions. A yield criterion involves coupled effect of the axial and circumferential internal force resultants is presented. Using a combination of power-law strain hardening, and strain rate hardening flow stress models, both strain hardening and strain rate effects are included. The intended method allows consideration of influence of various terms of kinetic energy and plastic work of the tube. The study presents a typical electromagnetic tube expansion model, using a dynamic high strain-rate forming method with strain-rates above  $10^3 \text{ s}^{-1}$ . Using the proposed method, the deformation of the specimen is achieved by the interaction of a current generated in the specimen with a magnetic field generated using a coil adjacent to the specimen. Results reveal that the achieved high strain rates influence the plastic flow stress and the final permanent radial deformation, consequently. The study concluded that an appropriate shape function eventuates a more accurate estimation of both the radial displacement and the deformed meridian profile.

**Keywords:** Electromagnetic forming, tube bulging, energy method, high strain-rate, thin cylindrical shell.

## 1 Introduction

Electromagnetic forming (EMF) method is a mechanical high-speed forming process which initially attracted scientists and consequently used as an advanced forming process in industries [1]. Utilizing pulsed magnetic pressure in a flexible and controllable manner, the process which can shape a metal workpiece into the desired geometry holds advantages in comparison with conventional processes, including improved forming limit, active-controlled spring back, and suppressed wrinkling [2].

Similar to other methods, some part of the external source energy absorbed by the workpiece is changed into the energy of plastic deformation, and the rest is transformed into kinetic energy [3], [4]. After the pulsed loading terminated, the workpiece is continuously deformed by its inertia force, until the kinetic energy completely changes into plastic work. As the forming procedure involves high frequency and high-powered

coupled circuits, which have electrical and geometric properties varying with time [5], Due to the coupling of highly nonlinear transient phenomena, it is a challenging practice to understand the EMF process comprehensively [1].

Mamalis et al. [6] gives a comprehensive review and assessment of the electromagnetic forming process and reports different methods that are mainly used in the analysis of the electric circuits in the EMF process. The equivalent circuit was developed and exemplified by Al-Hassani et al. [7] using a combined coil and the workpiece. The equivalent inductance and resistance are then represented as functions of both the coil and workpiece parameters. Correia et al. [8] compared the results obtained from Maxwell's equations in case of a stationary medium with those obtained for a moving medium. Using Manea et al. [9] research on different velocities ( $10^3$ ,  $10^5$ ,  $10^7$  m/s), Correia reports that electromagnetic field in a moving medium varies considerably less compared to the magnetic field in a stationary medium.

In case of a thin cylindrical shell which is subjected to a time-varying radial pressure, Hodge [10] reported some of such analytical approaches developed by different researchers. Applying the momentum equations to the finite shell portions separated by two hinges together with suitable movement compatibility conditions, other authors [11] proposed shell deformation patterns using fixed or moving plastic hinges.

Some researchers used finite element methods to analyse complex EMF processes with a loose coupling assumption [12], [13]. The proposed method assumes EMF process as two independent processes: electromagnetic field and plastic deformation. No mutual influence considered between the electromagnetic field and tube forming [14].

Due to the symmetry of the electromagnetic bulging process, an axisymmetric configuration has been used for both the workpiece and the coil. Hence, the magnetic field and the resulting magnetic pressure acting on the tube do not vary in the circumferential direction. Considering these assumptions, the problem reduces to the case of a thin cylindrical shell which is subjected to time-varying radial pressure.

Defining the structural part of the model based on the approach of [3] for plate deformation problem, the model presented here includes each of the following effects: translation and rotatory inertia, circumferential and longitudinal membrane forces, and longitudinal bending moment. To define the relation of both the internal resultant forces and the longitudinal bending moment with the displacement field, a new yield criterion is proposed. Involving the coupled effect of these internal force resultants, this criterion is adapted to the geometric situation under study.

## 2 Electromagnetic pressure

The mechanical model for axisymmetric tubular shells presented later is suited for pulsed loading. A typical application in forming technology, where such loads are applied to the geometries under consideration is EMF. To make the presentation more concrete, this application is considered and a model according to Al-Hassani [7] is resumed to compute the loading in this situation.

A typical magnetic forming procedure is shown schematically in Fig.1. The coil is looped on a rectangular bar in a strong insulating case. The field generated within the solenoid is retained in the gap between the coil and the tube.

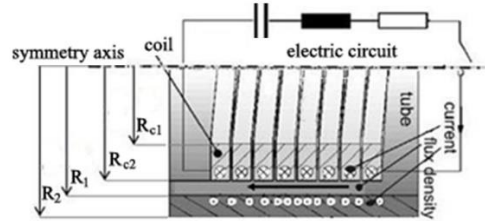


**Fig.1:** Schematic axisymmetric 2D representation of electromagnetic tube bulging. Image reproduced from Ref. [7]

With the aid of an equivalent circuit, Ref. [7] expressed the internal radial electromagnetic pressure for this condition as

$$p = \frac{\mu_0 i^2 N^2}{2} \left\{ \frac{R_{C1}^2}{r^2 - R_{C2}^2 + R_{C1}^2} \right\}^2 \quad (1)$$

where  $r$  is the deformed radii of the workpiece,  $R_{C1}$  and  $R_{C2}$  are the internal and external radius of the coil, respectively.  $N$  is the number of coils turns per meter and  $\mu_0$  is the permeability of free space ( $\mu_0 = 4\pi \times 10^{-7} H/m$ ).

$i \equiv i(t)$  is the discharge current which in the experiments is very close to an exponentially decaying sinusoid. Therefore, a general form is taken in the present work as:

$$i(t) = i_0 \sin\left(\frac{\pi t}{2t_0}\right) \exp\left(\ln(k) \left(\frac{t}{2t_0} - \frac{\ln(k)}{2}\right)\right) \quad (2)$$

where  $2t_0$  is the characteristic time of the current pulse,  $i_0$  is the electric current at  $t=t_0$ , and  $k$  is a decay parameter,  $k = -i(3t_0)/i_0$ . This general form is found to give a satisfactory fit to the experimentally measured data [15].

### 3 Analytical model

Consider the axisymmetric configuration of a  $2L$  length thin cylindrical shell subjected to uniformly distributed internal radial pressure with uniform boundary condition around its both ends shown in Fig.2.

Since the complexity of the problem is such as to rule out analytical formulation, some assumptions made upon developing approximate methods for computing permanent deformation. A starting assumption which allows analytical treatment of the problem is to idealize the material as rigid plastic. One consequence of this idealization is to neglect the material characteristics of elasticity.

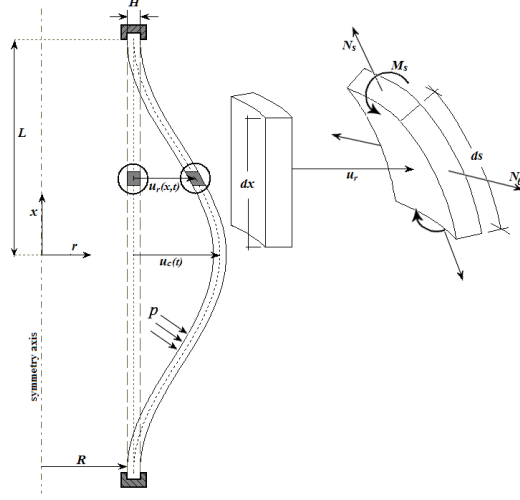


**Fig.2:** Meridian section and displacement field of a differential element of the shell

Therefore, the basic energy balance equation of the problem may be written as

$$\dot{W}_e = \dot{W}_p + \dot{E}_c \quad (3)$$

where  $\dot{W}_e$ ,  $\dot{E}_c$  and  $\dot{W}_p$  represent the rate of external load work, kinetic energy and energy dissipation by plastic deformation, respectively.

All these terms may be obtained from the displacement field at mid-plane points of the shell. This field may be described as the product of a function of time  $u_c(t)$ , representing the radial displacement of the  $x=0$  point of the shell wall, and a shape function  $\phi(x)$  of the axial distance  $x$  of the considered point:

$$u_r(x, t) = u_c(t) \cdot \phi(x) \quad (4)$$

As shown in Fig.2, a differential element of the shell which had the initial length  $dx$  and radial position  $R$ , deforms to the current radial position  $r$  and length  $ds$  which may be expressed as

$$r = R + u_r \quad (5)$$

$$ds = \sqrt{1 + u_c^2 \phi'^2} dx \quad (6)$$

### 3.1 External load work rate

If the boundaries remain fixed and no mechanical work is produced by boundary reactions, the only external work is the one done by the radial electromagnetic force. So, the external load work rate becomes

$$\dot{W}_e = \int_0^L \int_0^{2\pi} p \dot{u}_r r dx d\theta \quad (7)$$

where  $\dot{u}_r$  is the radial velocity of any point of the shell's mid surface at position  $x$  which may be expressed as  $\dot{u}_r = \dot{u}_c \cdot \phi$ . The pressure  $p$  is assumed to be uniformly distributed over the internal surface of the shell i.e.  $\partial p / \partial x = \partial p / \partial \theta = 0$ . Now, substituting Eqs.(5) and (6) into (7),

$$\dot{W}_e = 2\pi p \dot{u}_c \int_0^L (R + u_c \phi) \phi dx. \quad (8)$$

### 3.2 Kinetic energy rate

The kinetic energy rate of the shell may be considered as a summation of translational and rotational components:

$$\dot{E}_c = \dot{E}_c^t + \dot{E}_c^r \quad (9)$$

With the same procedure of the external load work rate, the rate of translational kinetic energy and rotational kinetic energy of the element shown in Fig.2 can be expressed as:

$$\dot{E}_c^t = 2\pi \rho H R \dot{u}_c \ddot{u}_c \int_0^L \phi^2 dx \quad (10)$$

$$\dot{E}_c^r = \frac{1}{6} \pi \rho H^3 R \int_0^L \frac{\dot{u}_c \ddot{u}_c \phi'^2 + u_c^2 \dot{u}_c \ddot{u}_c \phi'^4 - 2u_c \dot{u}_c^3 \phi'^4}{(1 + u_c^2 \phi'^2)^3} dx \quad (11)$$

where  $\ddot{u}_c$  represents the radial acceleration of the shell wall at  $x = 0$ .

### 3.3 Plastic work rate

When the thickness of the tube is small with respect to its diameter, a distribution of circumferential stresses is almost uniform. Then, the axisymmetric geometry of the tube and axisymmetric distributed internal pressure provide the zero circumferential bending moment condition in the tube wall. Therefore, referring to Fig.2, the plastic work in the shell may be obtained from the work of the following resultant forces and moment per unit length of the shell: the circumferential membrane force  $N_\theta$ , the longitudinal membrane force  $N_s$  and the longitudinal bending moment  $M_s$ . As the thickness of the shell is small in comparison to other dimensions, plastic work due to shear forces is neglected, leading to

$$\dot{W}_p = \dot{W}_p^{N_\theta} + \dot{W}_p^{N_s} + \dot{W}_p^{M_s} \quad (12)$$

The plastic work rate of these forces and moment can be written as follows:

$$\dot{W}_p^{N_\theta} = 2\pi \dot{u}_c \int_0^L N_\theta \phi \sqrt{1 + u_c^2 \phi'^2} dx \quad (13)$$

$$\dot{W}_p^{N_s} = 2\pi \dot{u}_c \int_0^L N_s \frac{(R + u_c \phi) u_c \phi'^2}{\sqrt{1 + u_c^2 \phi'^2}} dx \quad (14)$$

$$\dot{W}_p^{M_s} = 2\pi \dot{u}_c \int_0^L M_s (R + u_c \phi) \frac{\phi'' (u_c^2 \phi'^2 - 1)}{(1 + u_c^2 \phi'^2)^2} dx \quad (15)$$

To utilize the Eqs. (13), (14) and (15) in a displacement-based solution algorithm, the relation between the internal resultant forces and the displacement field should be obtained. Such relations can be obtained from the assumption that a suitable yield condition is fulfilled during the whole forming process. Therefore, the approach of Zaera et al. [3] for axisymmetric forming of thin metal plates is transferred to the geometric situation as:

$$\left( \frac{M_s}{M_p} \right)^2 + \left( \frac{N_s}{N_p} \right)^2 + \left( \frac{N_\theta}{N_p} \right)^2 - \frac{N_s N_\theta}{N_p^2} = 1 \quad (16)$$

where  $N_p = \sigma_y \cdot H$ , the fully plastic membrane force, is the magnitude of a force necessary to produce plastic flow over the entire wall thickness of a shell,  $M_p = \sigma_y \cdot H^2/4$ , the fully plastic bending moment, is the plastic capacity of the cross-section when subjected to a pure bending moment [11] and  $\sigma_y$  is the plastic flow stress. The new yield condition is validated by comparison to yield criteria reported in Ref. [10] and Ref. [11] in Fig.3.

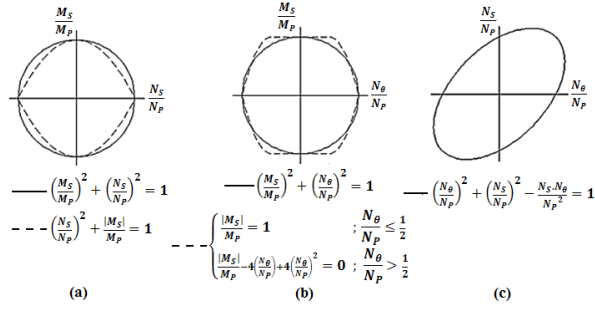


**Fig.3:** Comparison between the presented yield ellipsoid and other known yield criteria: (a) Yield ellipsoid intersection with  $N_\theta=0$ , (b) Yield ellipsoid intersection with  $N_s=0$ , (c) Yield ellipsoid intersection with  $M_s=0$ .

#### 4 Constitutive equation, resultant forces and bending moment

The normality rule of plasticity for the current problem may be expressed as

$$\frac{\dot{\epsilon}_\theta}{\left(\frac{\partial f}{\partial N_\theta}\right)} = \frac{\dot{\epsilon}_s}{\left(\frac{\partial f}{\partial N_s}\right)} = \frac{\dot{\kappa}_s}{\left(\frac{\partial f}{\partial M_s}\right)} \quad (17)$$

Using equation (17) and the yield criterion, the following expressions for the internal force resultants can be obtained:

$$M_s = \sqrt{3} \frac{M_p^2 \dot{\kappa}_s}{\sqrt{3M_p^2 \dot{\kappa}_s^2 + 4N_p^2 (\dot{\epsilon}_s^2 + \dot{\epsilon}_\theta^2 + \dot{\epsilon}_s \dot{\epsilon}_\theta)}} \quad (18)$$

$$N_s = \frac{2\sqrt{3}}{3} \frac{N_p^2 (2\dot{\epsilon}_s + \dot{\epsilon}_\theta)}{\sqrt{3M_p^2 \dot{\kappa}_s^2 + 4N_p^2 (\dot{\epsilon}_s^2 + \dot{\epsilon}_\theta^2 + \dot{\epsilon}_s \dot{\epsilon}_\theta)}} \quad (19)$$

$$N_\theta = \frac{2\sqrt{3}}{3} \frac{N_p^2 (2\dot{\epsilon}_\theta + \dot{\epsilon}_s)}{\sqrt{3M_p^2 \dot{\kappa}_s^2 + 4N_p^2 (\dot{\epsilon}_s^2 + \dot{\epsilon}_\theta^2 + \dot{\epsilon}_s \dot{\epsilon}_\theta)}} \quad (20)$$

There are various forms to relate the plastic flow stress to the plastic strain and strain rate. As an option, a combination of the well-known power-law strain hardening and strain rate hardening equation [15] can be used:

$$\sigma_y = (A \bar{\epsilon}^n) \left[ 1 + \left( \frac{\dot{\epsilon}}{\dot{\epsilon}_0} \right) \right]^{1/m} \quad (21)$$

where  $A$ ,  $n$ ,  $m$  and  $\dot{\epsilon}_0$  are material constants. Further,  $\dot{\epsilon}$  is effective strain rate which can be expressed by

$$\dot{\epsilon} = \sqrt{\frac{2}{3}(\dot{\epsilon}_s^2 + \dot{\epsilon}_\theta^2)} \quad (22)$$

Using the expressions obtained from the previous sections and the assumed displacement field (Eqn.(4)), the energy balance equation, given in Eqn.(3), may be rewritten finally as a differential equation containing the variable  $u_c$  and its derivatives:

$$F(u_c, \dot{u}_c, \ddot{u}_c) = 0 \quad (23)$$

This is a nonlinear ordinary differential equation whose coefficients depend on time and must be computed via integration in space. Therefore, this equation is discretized by constant-average-acceleration Newmark's scheme. The resulting algebraic equations for each time step are then iteratively solved by the Modified Newton-Raphson algorithm.

## 5 Results and discussion

To validate the model, an example has been analyzed: A tube consisting of the aluminum alloy *AA6063-T6*, longer than the forming coil simulated by Thomas et al. (2009) [15] is considered. Material properties of the tube, geometry and current parameters (Eqn.(2)) are listed in Table 1.

**Table 1:** Case study specifications

AA6063-T6 uniaxial mechanical constitutive parameter values [15]					
$E$ (Pa)	$\sigma_0$ (Pa)	$n$	$m$	$\dot{\epsilon}_0$ (s <sup>-1</sup> )	$\rho$ (kg/m <sup>3</sup> )
$69 \times 10^9$	$195 \times 10^6$	1/13.89	0.0870	1000	2700
Geometry of the tube and coil					
Tube			Coil		
$R_1$ (m)	0.02850	$R_{C1}$ (m)	0.02101		
$R_2$ (m)	0.03025	$R_{C2}$ (m)	0.02664		
$2L$ (m)	0.0851	$P_C$ (m)	0.0094		
		$2L_C$ (m)	0.03382		
Coil current parameters					
$i_0 = 137 \times 10^3$ A		$T_0 = 17 \times 10^{-6}$ s		$k = 0.3$	

With these values, the induced current in the coil is obtained. To complete the presented energy balance equation, a function  $\phi(x)$  must be defined. For this example, the function is proposed as:

$$\phi(x) = (1/2) \left[ 1 - \text{sign} \left( \left( |x|/L_e \right) - 1 \right) \right] \psi(x) \quad (24)$$

where  $L_e = 1.2L_C$  is the effective length of the tube and is defined as the maximum axial distance from the tube midline that may be affected by the radial electromagnetic force [16]. For the function  $\psi(x)$ , a variety of continuous functions could be considered, such as, e.g.,

$$\psi(x) = \begin{cases} \frac{1}{2}[1 + \cos(\pi x/L_e)] \\ \cos(\pi x/2L_e) \\ 1 - (x/L_e)^2 \\ 1 - (|x|/L_e)^3 \end{cases} \quad (25)$$

In Fig.4a the deformation profiles defined by these functions and compared to the experimental deformation profile. As can be seen,  $\psi_1(x) = (1/2)[1 + \cos(\pi x/L_e)]$  has the closest match with the experimental and other numerical results. This match can be seen in Fig.4b which shows the calculated circumferential strain of the tube midline during the process, using energy method and neglecting strain rate effects.

These two comparisons show the capability of the presented energy method in modelling the tube electromagnetic forming process and it can be concluded that the shape function  $\psi_1$  is the most appropriate one for this purpose.

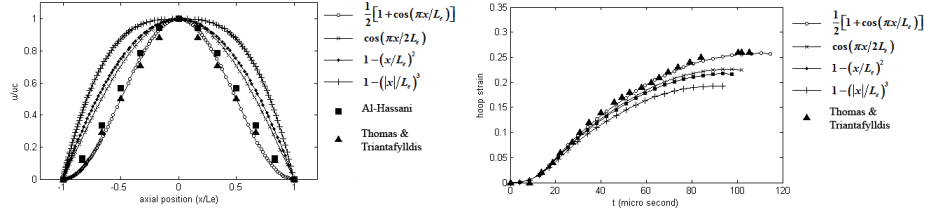


**Fig.4:** Comparison of the results computed with shape functions and experimental results; deformed profile (left) The variation of the tube's mid-surface at  $x=0$  (right)

The plastic behaviour of the material is affected by the high strain rate values. The calculated plastic flow stress and the displacement over the time of the tube's mid-surface at  $x=0$ , estimated by the viscoplastic material model, are plotted, and compared to those estimated with the rate-independent one. The difference between dynamic and quasi-static flow stress is obvious and as can be seen, this difference reaches the maximum (approximately about 40 MPa) after the first pressure peak. Besides, the higher the flow stress, the more plastic work is obtained for a certain displacement. Therefore, as indicated in Fig.5, the tube displacement value obtained from the viscoplastic model is significantly smaller than that obtained from the rate-independent model.

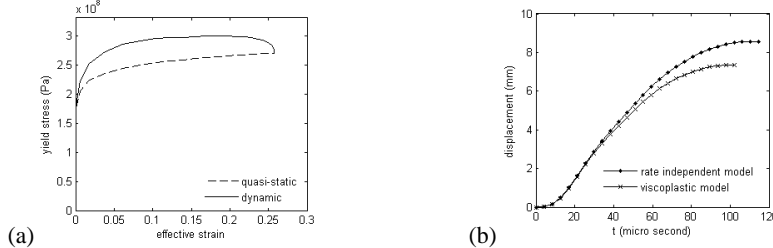


**Fig.5:** Comparison between viscoplastic (dynamic) and rate-independent (quasi-static) material models; (a) The plastic flow stress and (b) mid-surface at  $x=0$  displacement.

However, one of the main advantages of the presented model is that it allows a separate study of each internal component of the plastic work during the process. For instance, Fig.6 demonstrates normalized membrane forces and the normalized longitudinal bending moment at three different stages of the process. In all stages, the circumferential membrane force is more important than the other ones.

The behaviour of the longitudinal membrane force is different; at the earlier stages, the distribution of this force on the axial midline is uniform (along  $x$ ) tending to zero near the effective length. The value of this force increases with increasing the distance from the point  $x=0$  over time and its maximum occurs near the coil ends ( $x/L = 0.4$ ).

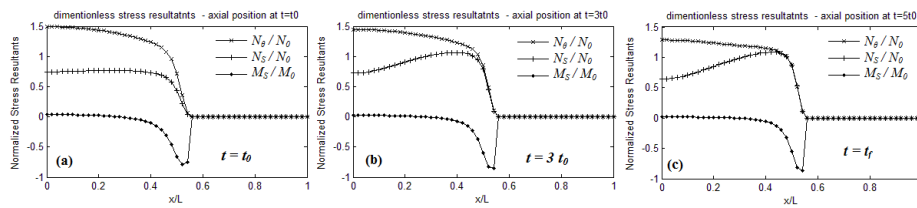


**Fig.6:** Diagrams of dimensionless internal force resultants at three different instances: (a)  $t=t_0$ , (b)  $t=3t_0$ , (c)  $t=t^f$  ( $t=t^f$  is the time in which the deformation of the workpiece ends)

## 6 Conclusion

Intended simplified analytical model of an electromagnetic bulging of thin metallic cylindrical tubes shown a close result to those obtained previous by numerical simulations. Considering energy balance equation, the model involves the coupled effect of the axial and circumferential internal forces and bending moment, including both strain hardening and high strain rate effects.

High strain rate values achieved through the process affect the plastic behaviour of the tube and the estimated displacements from a viscoplastic model are significantly less than those obtained from a rate-independent model.

The shape function  $\psi_1(x) = (1/2)[1 + \cos(\pi x/L_e)]$  yields the best approximations for both the tube's mid-surface at  $x=0$  displacement and deformed meridian profile. The current analytical simulation could be expanded to any axisymmetric shells, boundary conditions, and loading examples, considering right shape function.

## References

- [1] E. Paese, M. Geier, R. P. Homrich, P. Rosa and R. Rossi, "Sheet metal electromagnetic forming using a flat spiralcoil: experiments, modeling, and validation," *Journal of Materials Processing Technology*, pp. 408-422, 2019.
- [2] Z. Lai, Q. Cao, X. Han, M. Chen, N. Liu, X. Li, Q. Cao, Y. Huang, Q. Chen and L. Li, "Insight into analytical modeling of electromagnetic forming," *The International Journal of Advanced Manufacturing Technology*, p. 2585–2607, 2019.

- [3] R. Zaera, A. Arias and C. Navarro, "Analytical modelling of metallic circular plates subjected to impulsive loads," *Int J Solids Struct*, pp. 659-672, 2002.
- [4] F. Song, X. Zhang, Z. Wang and L. Yu, "A study of tube electromagnetic forming," *J Mater Process Technol*, p. 372-375, 2004.
- [5] G. Fenton and G. Daehn, "Modeling of electromagnetically sheet metal," *J Mater Process Technol*, pp. 6-16, 1998.
- [6] A. Mamalis, D. Manolakos, A. Kladas and A. Koumoutsos, "Electromagnetic forming and powder processing: Trends and developments," *Appl Mech Rev*, pp. 299-324, 2004.
- [7] S. Al-Hassani, J. Duncan and W. Johnson, "On the parameters of the magnetic forming process," *J Mech Eng. Sci*, pp. 1-9, 1974.
- [8] J. Correia, M. Siddiqui, S. Ahzi, S. Belouettar and R. Davies, "A simple model to simulate electromagnetic sheet free bulging process," *Int J Mech Sci*, pp. 1466-1475, 2008.
- [9] T. Manea, M. Veweij and H. Blok, "The importance of velocity term in the electromagnetic forming process," in *Proc Twenty seventh general assembly of the international union of radio science URSI*, Maastricht, 2002.
- [10] P. G. Hodge, *Limit analysis of rotationally symmetric plates*, NJ: Prentice-Hall, 1963.
- [11] N. Jones, *Structural Impact*. Cambridge University Press, Cambridge, 1997.
- [12] Y. Kiliclar, O. Demir, I. Vladimirov, L. Kwiatkowski, A. Brosius, S. Reese and A. Tekkaya, "Combined simulation of quasi-static deep drawing and electromagnetic forming by means of a coupled damage-viscoplasticity model at finite strains," in *The 5th International Conference on High Speed Forming*, Dortmund, 2012.
- [13] X. Cui, J. Mo, J. Li, J. Zhao, Y. Zhu, L. Huang and Z. Li, "Some recent researches employed the finite element method to analyze the complex EMF process with a loose coupling assumption. This method assumes the EMF process as two independent processes of electromagnetic analysis and deformation so does not take into account," *Journal of Materials Processing Technology*, pp. 409-427, 2014.
- [14] L. Qiu, Y. Xiao, C. Deng, Z. Li, Y. Xu, Z. Li and P. Chang, "Electromagnetic-structural analysis and improved loose coupling method in electromagnetic forming process," *The International Journal of Advanced Manufacturing Technology*, p. 701-710, 2017.
- [15] J. Thomas and N. Triantafyllidis, "On electromagnetic forming processes in finitely strained solids: Theory and examples," *J Mech Phys Solids*, pp. 1391-1416, 2009.
- [16] L. Zhong, L. Chun-feng, Y. Hai-ping and Z. Zhi-heng, "Effect of tube size on electromagnetic tube bulging," *Trans Nonferrous Met Soc China*, pp. 705-710, 2007.
- [17] S. Al-Hassani, "Electromagnetic metal forming processes. Dissertation," University of Manchester Institute of Science and Technology UMIST, Manchester, 1962.